POLITECNICO DI TORINO
Repository ISTITUZIONALE

Dynamic Machine Testing of Running Specific Prostheses Based on User-Specific Input Parameters

Original
Dynamic Machine Testing of Running Specific Prostheses Based on User-Specific Input Parameters / Barattini, C., Vigliani, A., Starker, F.. - In: EXPERIMENTAL TECHNIQUES. - ISSN 0732-8818. - ELETTRONICO. - 50:4(2026), pp. 587-598. [10.1007/s40799-025-00838-w]

Availability:
This version is available at: 11583/3003487 since: 2025-09-30T07:54:11Z

Publisher:
Springer Science and Business Media Deutschland GmbH

Published
DOI:10.1007/s40799-025-00838-w

Terms of use:

This article is made available under terms and conditions as specified in the corresponding bibliographic description in the repository

Publisher copyright

(Article begins on next page)

19 November 2026

Experimental Techniques (2026) 50:587–598
https://doi.org/10.1007/s40799-025-00838-w

RESEARCH PAPER

Dynamic Machine Testing of Running Specific Prostheses Based on User-Specific Input Parameters

C. Barattini[1] · A. Vigliani[1] · F. Starker[2]

Received: 17 April 2025 / Accepted: 25 August 2025 / Published online: 15 September 2025
© The Author(s) 2025

Abstract

This paper presents a new testing protocol for running-specific prostheses that aims to better simulate real running conditions. Unlike traditional methods that often use fixed conditions and lack standardization, this approach adjusts the rotation of the bottom platform and the vertical compression force, based on findings from treadmill tests and static analyses. The study tests two prosthetic footblade models by simulating two different running styles. To evaluate the accuracy of these dynamic tests, the study compares the vertical and horizontal forces measured during testing to those recorded from actual users running. The most accurate test showed only a 2.46% error in the ratio of horizontal to vertical forces and a 2.38% standard deviation compared to real-life data. These findings indicate that the testing method closely matches real-world conditions, demonstrating its reliability. In the future, this dynamic testing method could be standardized to improve the evaluation of prosthetic running blades across various models and stiffness levels, helping to bridge the gap between laboratory tests and real-world usage.

Keywords Machine testing · Running biomechanics · Machine simulation · Prosthetics · Stiffness

Nomenclature

$\bar{E}_1$	slope of the of the first 30% of the quasi-static loading curve
$\bar{E}_2$	slope of the of the remaining 70% of the quasi-static loading curve
$\hat{E}_1$	slope of the of the first 30% of the estimated quasi-static loading curve
$\hat{E}_2$	slope of the of the remaining 70% of the estimated quasi-static loading curve
F	load evaluated at the upper end of the prosthesis from the experimental running test data
$\bar{F}$	load measured at the load cell during the quasi-static tests
$\hat{F}$	estimated load for quasi-static tests when $\alpha \in [26°, 40°]$
$\tilde{F}$	load measured at the load cell during the dynamic machine tests
R	ground reaction force measured from the treadmill during experimental running tests
α	inclination angle of the machines' lower platform
θ	rotation of the prosthesis reference frame, in the sagittal plane, estimated from the experimental running tests
γ	inclination of the prosthetic pylon, attached to the prosthesis, during dynamic machine tests
$[*]^n$	interpolation point on loading curves, $n \in [1, 30]$
$[*]_\zeta$	horizontal direction component in the sagittal plane
$[*]_\xi$	vertical direction component in the sagittal plane
$[*]_y$	horizontal direction component in the prosthetic reference frame
$[*]_z$	vertical direction component in the prosthetic reference frame

✉ C. Barattini
claudia.barattini@polito.it

A. Vigliani
alessandro.vigliani@polito.it

F. Starker
fstarker@ossur.com

[1] Department of Mechanical and Aerospace Engineering, Politecnico di Torino, Corso Duca degli Abruzzi 24, 10129 Torino, Italy

[2] R&D, Össur, Grjótháls 5, 110 Reykjavík, Iceland

Introduction

Running Specific Prostheses (RSPs) are designed to allow for high-impact activities. To ensure optimal performance, it is essential to test prostheses in real-world conditions such as running [1, 2].

Extensive experimental analyses, primarily involving human subjects, have been conducted on the running biomechanics of amputees [3–8], typically associated using a simple spring-mass system. Therefore, the vertical stiffness of the affected and unaffected legs and of the prosthetic is usually computed. There are no standardized test specifications for experimental tests on RSPs, and various tools and methods are used for mechanical evaluations. This results in conflicting outcomes. For example, McGowan et al. [3] found that the stiffness of the affected leg decreased with speed, while Hobara et al. [4] measured a constant stiffness with speed. These differences may be due to variations in testing methods, the lower running speeds analyzed by Hobara et al., and the different RSP models used by the athletes. Rigney et al. [9] also demonstrated the necessity of developing a standard procedure. They performed experimental tests by adopting different marker locations on the amputated leg. They showed that motion capture techniques based on able-bodied methods produce different results compared to an amputee-specific approach. It was found that the RSP should not be analysed with just two markers, nor should the ankle joint be set at the same height as the biological ankle.

The stiffness properties of RSPs have also been widely evaluated through mechanical tests [1, 2, 10–13]. Machine testing offers the benefit of assessing the behaviour of prosthetics under different loads, stresses, and impact conditions, while ensuring the consistency and reproducibility of the data.

Machine testing protocols exist for assessing the properties of foot prostheses [14–17], with the aim for testing for cyclic fatigue testing assuming a walking gait. The development of a universal standard for running-specific prostheses remains highly challenging due to the intraindividual variability in running gait, influenced by individual biomechanics, running speed, and activity levels. In contrast, walking biomechanics is more extensively studied and understood.

While walking-based standards provide a foundation for evaluating prosthetic devices, they do not represent running motion. There is no standardised machine-based test to evaluate the functional behaviour of RSPs. As a result, studies rely on human testing in sports halls, which makes it challenging to set up all the necessary equipment. Simulating real-world running conditions on a machine would allow for a more controlled evaluation of functional performance. For this reason, researchers have attempted to replicate the running conditions that the prosthesis experiences in machine-based tests.

Usually, static tests are performed under mid-stance conditions since the maximum Ground Reaction Force (GRF) is measured, and the maximum stiffness can be recorded [1, 10]. However, as underlined by Beck et al. [10], the angle and force variations can cause different stiffness behaviours, which also depend on the shape of the test sample. From machine tests, Beck et al. [10] measured an increasing stiffness with load, in contrast with the experimental results of the in-field tests performed by McGowan et al. [3]. This difference is likely due to the prosthesis tilting during the stance phase of running, which leads to a decrease in stiffness.

Selecting the appropriate constraint for mechanical tests is crucial, as it directly impacts stiffness properties. Dyer et al. [2] suggested constraining the distal end during static tests to measure the highest stiffness, but this may result in over-constraining conditions. During running, the Force Contact Point (FCP) changes depending on multiple factors *i.e.,* speed, technique, straight or curved run and the fatigue of the athletes. Furthermore, the researchers wondered whether stiffness should be measured as an average value or at maximum load.

An experimental protocol has been proposed by Doyen et al. [11] to evaluate RSPs' performances. The experimental setup included a mechanical testing machine and a camera. The tests aim to evaluate the influence of the prosthesis-ground angle, the sole type and the flooring type on the prosthesis performances, in terms of secant stiffness and energy dissipation. However, this study faced limitations due to the displacement loading control, which prevented achieving the maximum force recorded during the run, as well as the constant relative angle between the prosthetic and the ground.

Mechanical tests are also relevant for the verification and validation of Finite Element (FE) models of prostheses [12, 18]. Rigney et al. [12] integrated the static and stress-relaxation tests with FE analyses to evaluate a reliable model, tuning the isotropic material properties, friction coefficient and Railegh parameters. Alternatively, Barattini et al. [18], optimised the orthotopic material properties of a FE model based on experimental hammer test results on the prosthesis.

The evaluation of prosthesis performance has also been conducted through modal tests by Noroozi et al. [13, 19, 20]. According to Noroozi et al.[13], once the stiffness is known, assuming fixed boundary conditions, the natural frequency can be predicted based on the mass applied, and the athletic bouncing movement can be adjusted to match the natural frequency of the prosthetic. Nonetheless, boundary conditions, such as the FCP, are variable and continuously change during running.

Other studies have focused on assessing the energy return properties of prostheses through drop tests [1, 21]. Notably, Grobler et al. [21] performed these tests on the combined assembly of the prosthetic and socket.

The varying approaches and conflicting results observed among researchers in evaluating RSPs stem from the lack of standardised criteria for assessing these devices under the specific conditions in which they are meant to be used.

It is important to underline, however, that mechanical testing cannot fully reproduce the conditions experienced during actual running. The movement of the whole body, the muscle control of the user and the high-speed movements cannot be replicated in a machine-based setup. Nevertheless, careful design of the mechanical testing protocol can improve the relevance of the test and provide meaningful insights into the functional performance of running-specific prostheses.

This paper presents the methodology for designing a machine dynamic test that mimics real-world running gait, while acknowledging the limitations discussed above. The tests are performed on two models, Cheetah® Xceed (CX) and Flex Run™(FR) (Össur hf. Iceland).

This study builds on ISO/TS 16955 [15] to develop an adapted setup for evaluating real-world running gait conditions. ISO/TS 16955 focuses on the performance characterization of walking feet of a specific size (260 mm height), for a specific intended user weight (70 kg). In contrast, this research aims to evaluate functional data using abstract running input profiles.

As underlined by the literature review, RSPs are typically tested using quasi-static, modal, or drop tests. In these analyses, the contact point and the relative rotation between the prosthetic component and the contact surface are usually fixed or uncontrolled, introducing a simplification in the tests that do not reflect real-world conditions. In contrast, this research aims to replicate the running gait conditions the prosthesis experiences on a dynamic machine by controlling the vertical compression load and the rotation of the contact platform.

The paper is organised as follows: in Section "Dynamic Test Setup and Tested Components", the experimental setup adopted for the dynamic tests is presented. Afterwards, the process for evaluating the input data for the tests is described and divided into four subsections. In Section "Running Gait Data", the post-processing of the running gait data obtained from the experimental running tests is outlined. In Section "Quasi-static Tests", the quasi-static tests performed are detailed. In Sections "Correlation of Real-life Running and Quasi-static Test Results" and "Input Data for the Dynamic Tests", the methodology for obtaining the input data is explained. Finally, in Section "Dynamic Tests", the results of the dynamic tests are presented. To conclude, in Section "Conclusions", considerations on the results and possible future developments are drawn.

Dynamic Test Setup and Tested Components

The RSP foot is tested in an adapted setup similar to the test specification ISO/TS 16955 [15], Fig. 1. According to the specifications, the load cell should be positioned at 0.5 m from the lower platform, which supposedly represents the location of a knee joint, while a pivot joint is set above the load cell at 0.7 m. These measurements correspond to dimensions h and H in Fig. 1 and are considered in the dynamic test setup.

The load cell used for the tests is a 6-Axis Combined Force/Torque (FT) sensor.

The parameters that are set and controlled during the dynamic test are the vertical input force above the pivot joint and the rotation of the tilt table (R_ξ and α in Fig. 1).

Choosing the right input settings and the output measurements is key to getting accurate and useful test results.

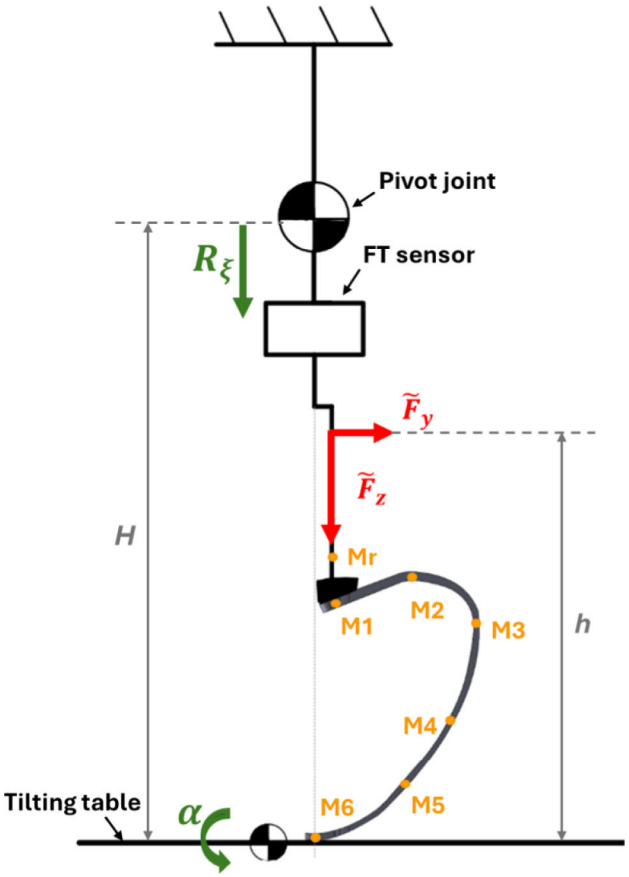


Fig. 1 Schematic representation of dynamic machine test. The test input data, R_ξ and α, are shown in green, while the measured loads, $\tilde{F}_y$ and $\tilde{F}_z$, are displayed in red. The markers' positions and nomenclature are highlighted in yellow. Six markers, from M_1 to M_6, are placed on the prosthesis, while M_r is located on the prosthetic pylon attached to the tested component



Fig. 2 Tested prosthesis models: Flex Run (a) and Cheetah Xceed (b). Photos ©Össur [24, 25]

In the stance phase simulation, the tilt table angle in the machine test setup does not directly match the shank tilting angle during running. This is because the prosthetic pylon can freely rotate under compression. This means that the Anterior/Posterior (A/P) forces observed are due to the mechanical behaviour of the RSP.

The input vertical force selected is the load measured from the force platform during the experimental running tests described in Section "Running Gait Data".

The validation parameter selected is the A/P force at the upper end of the prosthesis (F_y in Fig. 4). As the load cell is integrated in the setup under the pivot joint, it rotates together with the prosthetic pylon attached to the prosthesis. Hence, the horizontal force $\tilde{F}_y$ sensed by the FT sensor is rotating with the prosthetic upper part. Another option would be to measure the moment and compare it with the one sensed at the knee during running. However, knee joint height varies, and different methods can be used to measure the moment, such as Wearable Inertial Measurement Units (IMUs) or inverse dynamics based on motion capture and force plate data [22, 23]. These differences directly affect the resulting values.

During the tests, the deformation of the prostheses and the inclination of the prosthetic pylon are tracked using markers, which are represented in yellow in Fig. 1.

Since the main running movement occurs in the sagittal plane, for these tests, all considerations and computations are performed in this plane, without considering the lateral dimension.

Two different prosthesis models are tested: Cheetah® Xceed and Flex Run™, Össur hf. Iceland (Fig. 2). The first model is designed for sprinting purposes, while the other is developed for jogging and distance running. Table 1 providesan overview of the components tested, with their stiffness properties and the corresponding suggested user weight according to the Instructions For Use (IFUs). As stated in the table, both samples belong to the same stiffness category.

Dynamic Tests Pre-Processing

Figure 3 presents a schematic representation of the procedure followed during the pre-processing steps.

Firstly, the running test data, described in Section "Running Gait Data", are post-processed. During this step, the components of the GRF, R_ζ and R_ξ, the shank inclination θ and the components of the force in the Prosthesis Reference Frame (PRF), F_y and F_z, are evaluated (refer to Fig. 4). In particular, 30 values F_z^n and corresponding F_y^n are selected. The details of this process are outlined in Section "Running Gait Data".

Next, quasi-static tests at fixed inclination α of the contact platform have been conducted. This step, presented in Section "Quasi-static Tests", aims to evaluate the rotation angle of the tilt table for the dynamic test. Each prosthesis undergoes multiple tests, where α is changed for every trial. The forces at the load cell, $\bar{F}_{y,\alpha}$ and $\bar{F}_{z,\alpha}$, are collected.

Finally, the input data for the machine dynamic tests are evaluated, as outlined in Section "Input Data for the Dynamic Tests". For the vertical compression force, the load R_ξ, obtained from the post-processing of the treadmill running

Table 1 Tested components for the dynamic test

Model	Category	User mass [kg]	Naming
Cheetah Xceed	2	53 - 59	CX
Flex Run	2	45 - 52	FR

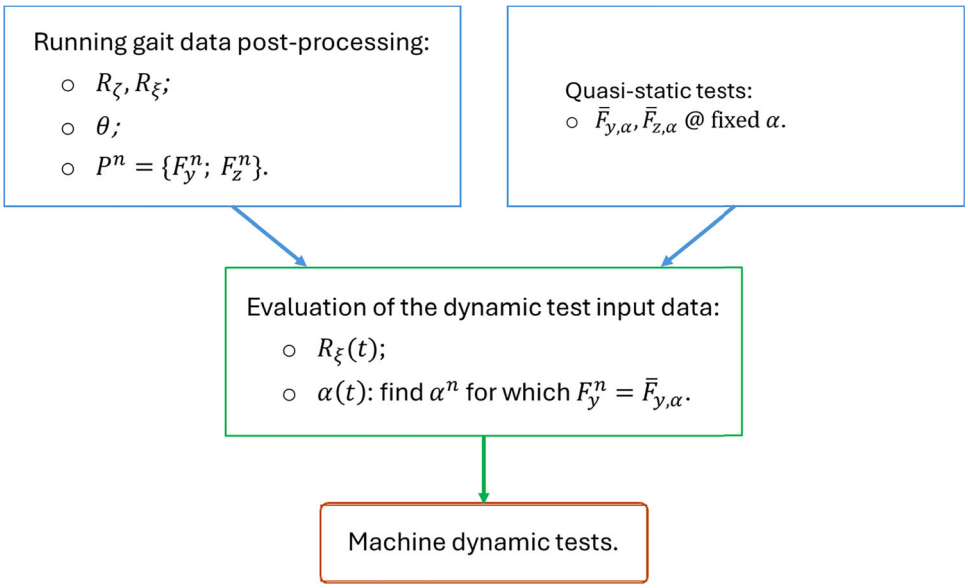


Fig. 3 Schematic of the workflow adopted to evaluate the input angles for the dynamic test, starting from the quasi-static tests and the running gait data

test data, is interpolated. The input rotation angle of the tilt table is instead evaluated from the comparison of the post-processed data of the experimental running tests (F_y^n) and the load recorded in the quasi-static tests ($\bar{F}_y$) at a specific inclination of the contact platform α.

Running Gait Data

The input running gait data is derived from experimental running tests conducted at Össur on two unilateral amputees running on a treadmill. During the tests, contact force and body movement were measured using force plates and a marker-based motion capture system.

User 1 is 1.65 m tall, weighs 66 kg, and has reduced knee joint mobility due to rotationplasty (RP). User 2 is 1.85 m tall, weighs 78 kg, and has a transtibial (TT) amputation. Both users wore the CX model in the stiffness category recommended by the manufacturer for their respective body mass.

Due to discrepancies in knee joint mobility, the biomechanics between the two users differ. The data considered corresponds to the top speed, which is 5.5 m/s for User 1 and 6.0 m/s for User 2.

The force at the location of the foot adapter, F, is computed from the GRF, R, evaluated during the experimental running tests. To ensure comparability with the forces measured at the load cell, the projections of F in the PRF, F_y and F_z, are computed. During the run, the PRF rotates according to the shank Center of Stability (CoS). Therefore, from the static force plate on the ground, the forces are calculated in the dynamic foot adapter CoS.

In Fig. 4, a schematic representation of the aforementioned parameters, along with the fixed ($\zeta\xi$) and prosthetic (yz) reference frames, is provided. The depiction of moments, however, is omitted. As displayed in the image, for the equilibrium of the prosthesis, the force at the upper end, F, must be equal in magnitude and opposite in direction to the GRF R.

As presented in Fig. 5, the PRF inclination θ, defined by the shank rotation, is higher for User 2, indicating that User 1's running gait involves a more horizontal landing on the blade.

The plots (b) and (c) of Fig. 5 show the GRF components, R_ζ and R_ξ, and the load components in the PRF, F_y and F_z. In the plots, the positive values of the force components correspond to the versus of the arrows displayed in Fig. 4. All the plotted variables are normalized over the percentage of the stance phase to eliminate the time basis for better comparability.

The vertical load R_ξ and the A/P force component in the PRF, F_y, are considered as input and output variables of the machine dynamic test. R_ξ is applied at the pivot joint, while F_y is the target to be sensed at the load cell during the dynamic machine test.

All the force data are averaged over the stance phases and normalized by the users' BodyWeight (BW), resulting in units of [N/BW]. For the machine tests, the input force values are subsequently multiplied by the BW intended for each stiffness category by the manufacturers IFU guidelines [26].

As expected, User 1 shows a higher vertical force and a lower A/P force in the PRF than User 2, since User 1 leans more forward during the run.

Figure 6 presents the relation between the vertical and horizontal force components in the PRF. On these curves, 30 points $P^n(F_z^n; F_y^n)$, where $n = 1, 2, ..., 30$, homogeneously spaced over the stance phase, are identified. These values are

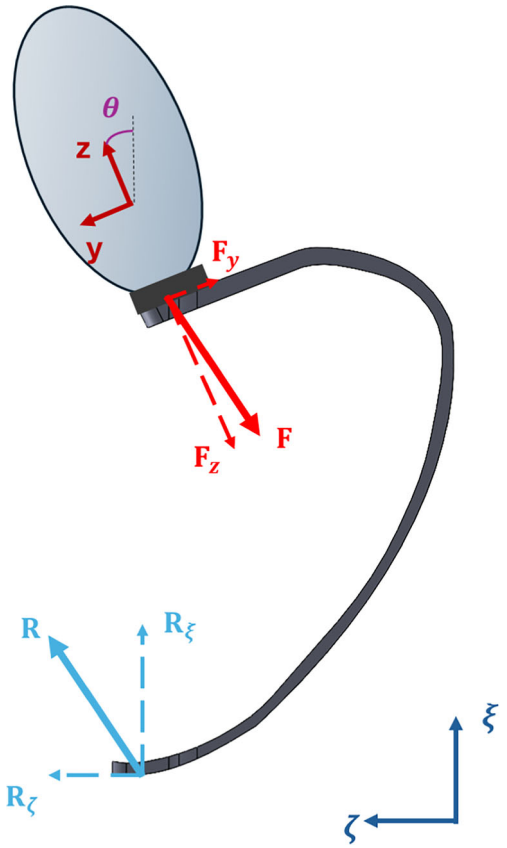


Fig. 4 Schematic representation of the ground contact force R and of the force at the upper distal end F. The projections R_ζ and R_ξ are measured in the absolute reference frame ($\zeta\xi$ plane) from the force platform, while F_y and F_z are the projections of F in the prosthesis reference frame, yz, which is defined by the shank inclination (θ). Here, the representation of moments is omitted

used to calculate the input vertical force and the A/P force as an output value, necessary for evaluating the input platform inclination in the dynamic test (Section "Quasi-static Tests").

Quasi-static Tests

As a preliminary analysis, quasi-static tests are performed on all the prostheses to evaluate the ideal inclination angle of the bottom platform for the dynamic machine tests based on the A/P force.

Both setups selected for static and dynamic testing do not differ despite a controlled moving bottom platform: the FT sensor is placed at 0.5 m from the bottom platform and is free to rotate in the sagittal plane due to the presence of a pivot joint at a height of 0.7 m.

The prostheses are placed on the machine considering the alignment suggestions of the guidelines [26]. Each component is tested for multiple tilt angles of the lower platform: $\alpha = -7°, -6°, -4°, -3°, 0°, 5°, \pm 10°, \pm 15°, \pm 20°, 23°, 24°$.

The prostheses tested are compressed with a vertical force to a maximum force of 3 times the intended user BW prescribed for that stiffness category [26]. Indeed, according to the vertical GRF measured in the running tests from the treadmill and supported by literature [3, 27], the maximum vertical force during running is approximately three times the body weight.

In Fig. 7, the vertical and horizontal forces measured at the load cell, in the sagittal plane, during one quasi-static test are displayed. For better viewing purposes, only the tests conducted at platform angles of $-20°$, $0°$, and $20°$ are shown. For zero and positive angles of the lower platform, which represent the toe-off condition in the running gait, CX showed around the 6% to the 20% higher horizontal force than FR, resulting in greater push forward.

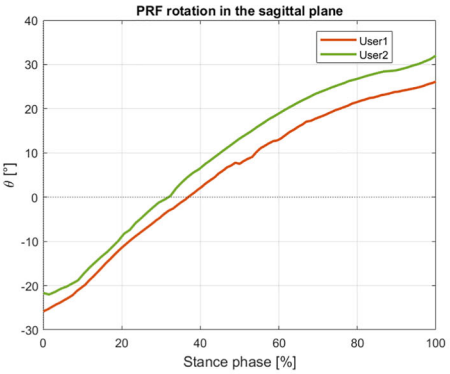
The circular markers in Fig. 7 (a) are the points where $\bar{F}_{z,\alpha} = F_z^n$. They represent the interpolation of 30 F_z^n values from the running-gait data onto the load cell curve. The corresponding $\bar{F}_{y,\alpha}^n$ values are determined from these points. Given the presence of hysteresis [10], the loading and unloading curves do not perfectly overlap. The loading curve is used to interpolate the F_z^n values related to the running phase from touch-down to mid-stance, while the unloading curve is used to simulate the next part of the run till take-off.

Based on the loading curves, it is verified that the correlation between $\bar{F}_{z,\alpha}$ and $\bar{F}_{y,\alpha}$ can be approximated as linear by dividing the curve into two segments: the initial 30% and the remaining 70% of the curve (Fig. 7 (b)). This holds true considering that the foot blades experience vertical loads up to three times the user's weight recommended for the specified stiffness category.

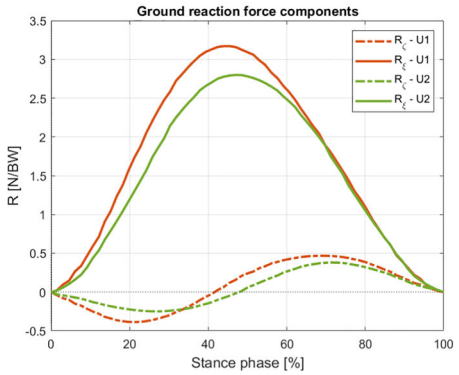
Correlation of Real-life Running and Quasi-static Test Results

To evaluate the input angle for the machine dynamic tests, the real-life running forces in the PRF are compared with those measured by the FT sensor during the quasi-static tests. The 30 F_z^n values, selected from the running gait data, are interpolated on the quasi-static curves to determine the corresponding $\bar{F}_{y,\alpha}^n$ values, as explained in Section "Quasi-static Tests" Fig. 7. For each F_z^n, meaning for each row, the platform inclination for which $\bar{F}_{y,\alpha}^n = F_y^n$ is selected.

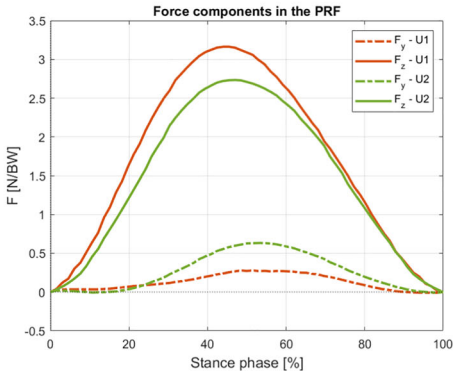
Since the quasi-static tests are performed up to a platform inclination of 24°, the horizontal force for higher inclinations, $\hat{F}_{y,\alpha}^n$, is estimated using linear interpolation, as given by Equation (1). This equation is based on the observation, performed in Section "Quasi-static Tests", that the relationship between $\bar{F}_z^n$ and $\bar{F}_y^n$ can be approximated as linear in two distinct regions: the first 30% and the remaining 70% (Fig. 7). To estimate the coordinates of the point at the 30% of the loading curve for inclination angles above 24°, it is assumed that the maximum vertical load sensed from the



(a)

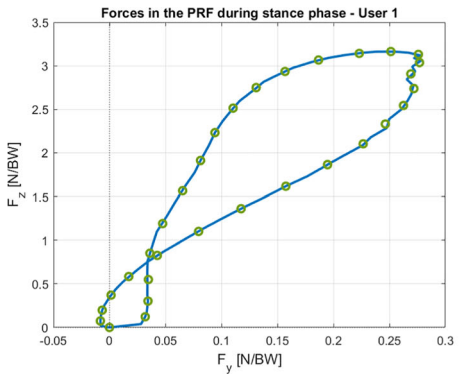


(b)

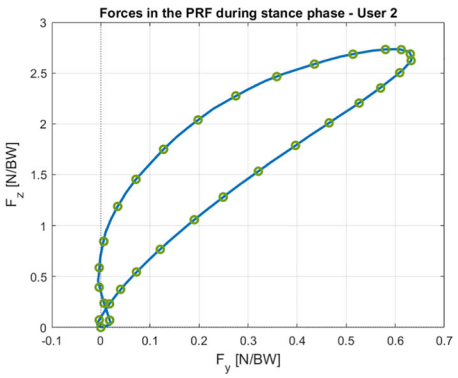


(c)

Fig. 5 Plots of the PRF rotation angle θ, vertical G components, R_ζ and R_ξ, and the load components in the PRF, F_y and F_z, over the running stance phase. The red and green curves present the running data of User 1 (U1) and User 2 (U2)

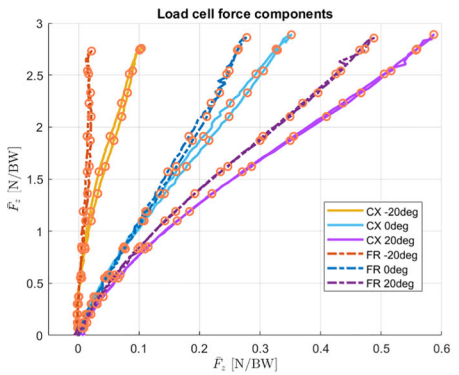


(a)

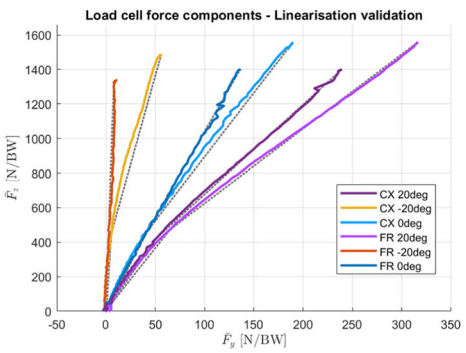


(b)

Fig. 6 Ground force components in the PRF scaled by the users' body weight. The 2D space of the sagittal plane is considered. The circular markers on the curve are the 30 points P^n selected as a reference for the next evaluations for the dynamic machine tests



(a)



(b)

Fig. 7 Forces measured at the FT sensor during the quasi-static tests on CX and FR, for platform inclination of $-20°$, $0°$ and $20°$. In plot (a), the loading unloading curves with the interpolation points are displayed (orange circles). In plot (b), the slopes of the loading curves are shown with dashed grey lines

load cell remains approximately the same as when $\alpha = 24°$. Thus, the vertical load is $0.3 \max(\bar{F}_{z,24°})$ for $\alpha \geq 24°$, and the corresponding horizontal load is calculated using Equation (3).

Consequently, the slope of the first part of the curve $E_{1,\alpha}$ and that of the subsequent part $E_{2,\alpha}$ are computed for each loading test, corresponding to different platform inclinations α.

To get the slopes for higher angles ($\hat{E}_{1,\alpha}$ and $\hat{E}_{2,\alpha}$), another linear interpolation is performed based on the slopes evaluated for tests at $\alpha = 20°$ and $\alpha = 24°$ (equation (4)). Once the new slopes are computed, approximated values of $\hat{F}^n_{y,\alpha}$, when $\alpha > 24°$ can be evaluated according to Equation (1).

The logic described above can be synthesised in the following list of passages:

1. compute $\bar{E}_{1,\alpha}$ and $\bar{E}_{2,\alpha}$ of the quasi static loading curves $\bar{F}_{y,\alpha}$ vs $\bar{F}_{z,\alpha}$ for every $\alpha \in [-20°, 24°]$;
2. evaluate $\hat{E}_{1,\alpha}$ and $\hat{E}_{2,\alpha}$ for $\alpha \in [26°, 40°]$ according to Equation (4);
3. estimate the coordinates $\hat{F}_{z,30\%}$ and $\hat{F}_{y,\alpha}\Big|_{\hat{F}_{z,30\%}}$ of the point at 30% of the loading curve for $\alpha \in [26°, 40°]$ (equations (2) and (3));
4. calculate $\hat{F}^n_{y,\alpha}$ for $\alpha \in [26°, 40°]$ and $n \in [1, 30]$ (equation (1)).

$$\hat{F}^n_y = \frac{F_z - \hat{F}_{z,30\%}}{E_{2,\alpha}} + \hat{F}_{y,\alpha}\Big|_{\hat{F}_{z,30\%}} \tag{1}$$

where:

$$\hat{F}_{z,30\%} = 0.3 \max\left(\bar{F}_{z,24°}\right) \tag{2}$$

$$\hat{F}_{y,\alpha}\Big|_{\hat{F}_{z,30\%}} = \frac{\hat{F}_{z,30\%}}{\hat{E}_{1,\alpha}} \tag{3}$$

$$\hat{E}_{g,\alpha} = \bar{E}_{g,24°} - \frac{\bar{E}_{g,24°} - \bar{E}_{g,20°}}{24° - 20°}(24° - \alpha), \text{ for } g = 1, 2 \text{ and } \alpha \in [26°, 40°] \tag{4}$$

Since the tilt angles considered are a limited number, linear interpolations are performed between the two closest values of $\bar{F}^n_{y,\alpha}$ to $F_{y,n}$ to determine the final output angle for the dynamic test, as given by Equation (5). In the equation, $\bar{F}^n_{y,h}$ is the nearest higher value to F^n_y, with α^n_h being the associated platform inclination. On the other hand, $\bar{F}^n_{y,l}$ refers to the closest lower value to F^n_y and α^n_l to the corresponding platform angle. For clarity, the equation only shows $\bar{F}^n_{y,h}$ and $\bar{F}^n_{z,h}$. However, the interpolated values of $\bar{F}^n_{y,h}$ and $\bar{F}^n_{z,h}$ are also taken into account, so that $\alpha \in [-20°, 40°]$.

$$\alpha^n = \frac{\alpha^n_h - \alpha^n_l}{\bar{F}^n_{y,h} - \bar{F}^n_{y,l}}(F^n_y - \bar{F}^n_{y,h}) + \alpha^n_h \tag{5}$$

The evaluations performed with the workflow presented, show that the trend of the input platform rotation varies among the tested prostheses.

Input Data for the Dynamic Tests

The dynamic tests are conducted using a hyrdaulic test machine (Shore Western KS-07) intended for endurance testing of prosthetic feet. Vertical loads are applied to the test samples via a linear piston at variable lower plate angles. The equipment operates at a maximum speed of 1500 mm/s with displacement adjusted by optimizing the vertical force input-to-output curves using PID loop control at 1000 Hz.

The machine's limited speed and responsiveness prevent an accurate simulation of human running. As a result, each loading cycle on the machine is adjusted to 2 seconds, about twice the length of actual running conditions. Within this cycle, the contact phase is set to $1s$, representing the stance phase of running, while the component remains out of contact for the next $1s$. As a result, input values for the dynamic tests are defined over $2s$ with a time discretisation of $0.001s$.

The input vertical compression force of the contact phase corresponds to the R_ξ force sensed from the treadmill during the running experimental tests (Fig. 5). As mentioned previously, the value in [N/BW] is used to eliminate the influence of individual user body mass. This value is normalised over the stance phase and scaled by the body mass recommended for each prosthetic stiffness category.

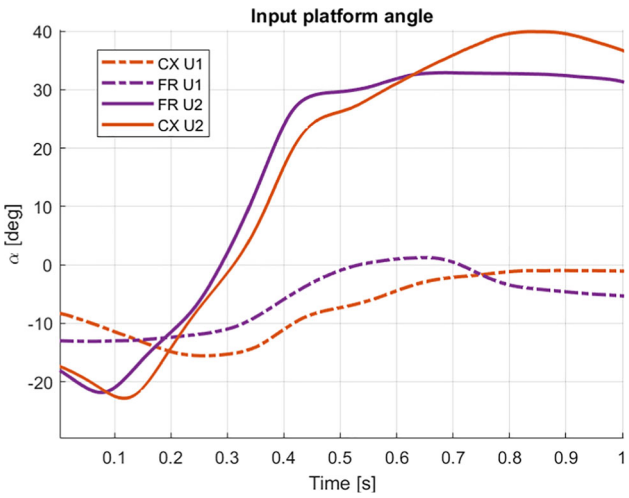


Fig. 8 Trend of the platform inclination angle selected for the dynamic tests for CX category 2 (red curves) and FR category 2 (violet curves) to simulate User 1's (dashed lines) and User 2's (continuous lines) run. Negative angle values refer to a dorsiflexed position

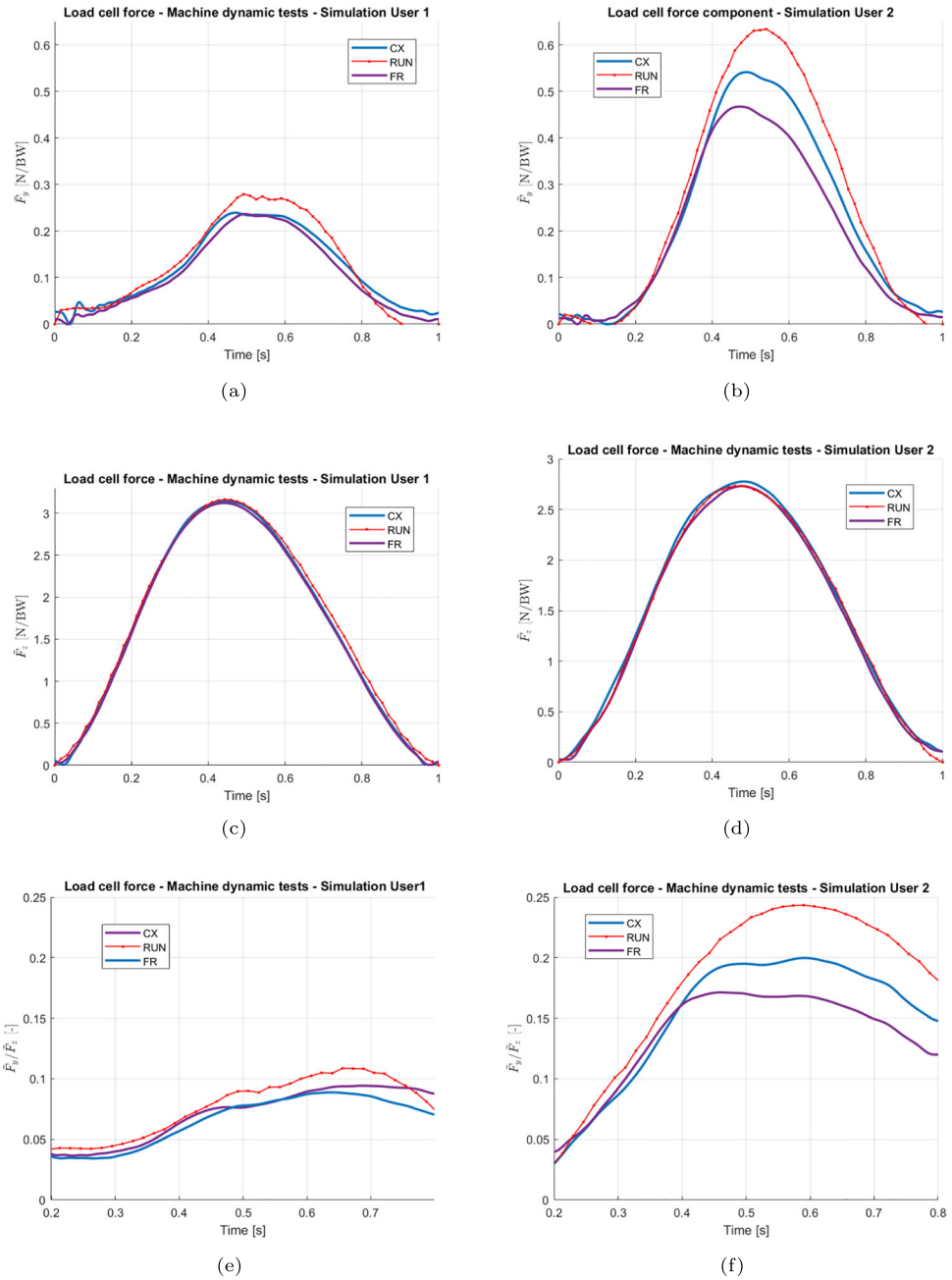


Fig. 9 Forces measured at the load cell during the dynamic tests. The results of loading CX categories 2 and FR category 2 are considered. Plots of the horizontal $\tilde{F}_y$ force component for the simulation of User 1's (a) and User 2's (b) run and of the vertical $\tilde{F}_z$ force component to mimic User 1's (c) and User 2's (d) run. Plots of the relation between force components sensed by the load cell for the simulation of U1 (e) and U2 (f)

To define the angle position at each time step of the stance phase simulation on the dynamic machine, an interpolation of the 30 α^n previously evaluated (Section "Correlation of Real-life Running and Quasi-static Test Results") is performed. Consequently, the time trend is extrapolated, and the platform rotation is defined for each time step up to $1s$. For the remaining part of the dynamic cycle, the platform moves linearly from the last position to the initial one of the next cycle.

An example of the platform rotation input values is plotted in Fig. 8. For the simulation of User 1's run, the platform inclination ranges from $-25°$ to $4°$, replicating a more dorsiflexed position. On the other hand, the range of rotation specified for the simulation of User 2's run is higher, moving from a minimum of $-25°$ to a maximum of $40°$. By following the process described in Section "Correlation of Real-life Running and Quasi-static Test Results", the input angle derived for simulating User 2's run with CX exceeds $40°$, however it is limited to this value. This restriction is necessary due to the piston's maximum travel range and the risk of slippage at higher inclinations, which can cause sudden detachment and require test abortion.

Table 2 Test results for Cheetah Xceed and Flex Run models when the User1's and User2's runs are simulated

Model	User	RMSE [%]	MAE [%]	R^2 [%]	σ [%]
CX	U1	2.46	2.11	90.36	2.38
FR	U1	2.93	2.58	86.74	2.18
CX	U2	3.26	2.42	97.67	2.99
FR	U2	9.61	6.94	67.90	7.40

The values of Root Mean Square Error (RMSE), the Mean Absolute Error (MEA), Coefficient of Determination (R^2) and standard deviation (σ) are reported for the error on $\tilde{F}_y/\tilde{F}_z$ between the dynamic tests and the real-life running gait data

Dynamic Tests

The dynamic tests are conducted by transferring the setup from the quasi-static testing machine to the dynamic machine, ensuring all setup variables remain constant. The input platform rotation angle computed for each model, α_{cx} and α_{fr}, is applied during the dynamic tests.

In Fig. 9, the vertical $\tilde{F}_z$ and horizontal $\tilde{F}_y$ forces measured by the load cell during the dynamic test are compared to the target, F_y and F_z, corresponding to the red curve called RUN.

Table 2 shows the correlation between the $\tilde{F}_y/\tilde{F}_z$ results from dynamic tests with real-life running gait data (F_y/F_z). Both prosthesis models successfully simulate User 1's running gait, with CX achieving the highest accuracy, as indicated by the lowest RMSE and MAE and highest R^2. For User 2, CX maintains a strong correlation (high R^2) but exhibits higher errors, while FR shows the highest errors and lowest correlation.

During the tests, markers were placed at the tested components and the attached prosthetic pylon, as shown in Fig. 1. From the post-processing of the videos, the deformation of the components and the rod inclination during the loading phase are evaluated. The rotation of the prosthetic pylon is tracked, its range of motion is found to be within [0, 10°]. Figure 10 compares the elastic deformation and prosthetic pylon inclination of CX and FR. For the same tested component, both parameters do not change significantly between User 1's and User 2's run simulations, despite the significant difference in the input lower platform inclination. The distal end displacement of the RSP differs by about 18% in the FR model and 25% in the CX model, while other markers show discrepancies of 0% to 5%. For pylon inclination, the discrepancy is 3% for CX and 7% for FR.

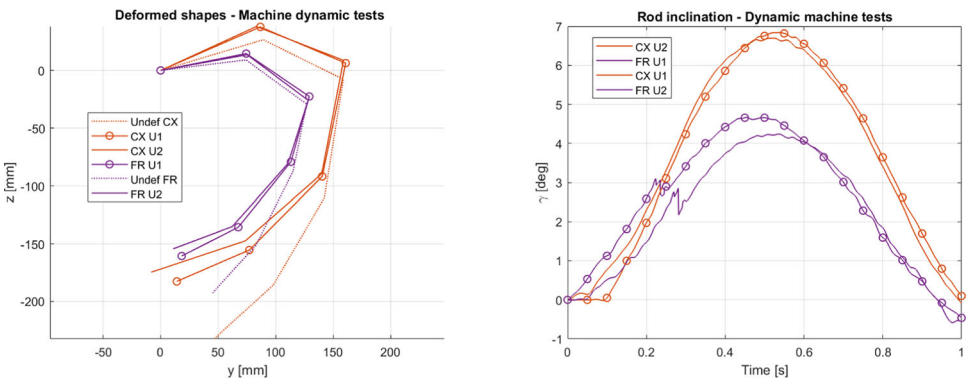
On the other hand, higher prosthetic pylon inclination is registered when CX is compressed. This is because the upper distal end (M1 in Fig. 1), located in the loaded region, displaces further downwards than the adjacent points, M2 and M3, compared to the FR model. The direct consequence of the greater prosthetic pylon inclination is a higher horizontal force component, $\tilde{F}_y$, in the CX model relative to the FR model, as previously mentioned and shown in Fig. 9(a) and (b). Moreover, even though a higher R_ξ is applied in simulating User 1, the displacement of the prostheses' lower distal end is bigger when User 2's run is simulated. This is a result of the higher platform angle applied.

Conclusions

The entire process to simulate the running gait on a dynamic machine, where the vertical force and the lower platform rotation angle can be controlled, is presented. The procedure involves post-processing real-world running gait data, conducting quasi-static tests on all the prosthesis samples, and comparing the results from these two steps to determine the input data for the dynamic test.

In this case, the specific running gait at high speed of two users is considered. Indeed, there are no standardised references for running gait, as factors such as speed, technique, and terrain affect both the gait pattern and the forces exerted on the prosthesis. As a result, empirical data must be used.

The two simulated running gaits have different characteristics. User 1 lands more horizontally on the blade while running due to limited knee joint mobility.



(a) (b)

Fig. 10 Deformation of the prostheses (a) and prosthetic pylon inclination (b) during the dynamic compression tests of CX and FR, category 2, for the simulation of U1 and U2 runs

Given the manufacturers' specifications, it is expected the model CX to better replicate the high-speed running conditions simulated in the machine tests compared to the FR. The FR is suitable for high-impact activities like recreational jogging and long-distance running, in contrast, CX is designed to maximise energy storage and return, which is essential when higher power is applied, such as during sprinting and jumping.

User 1's specific running motion could better be reproduced by the test setup compared to User 2. This may be related to the fact that, to simulate User 2, higher rotation angles are computed during the pre-processing steps. However, machine constraints only allow for an angle of 40°. In these tests, the same type of sole is used to avoid any difference in sole behaviour and friction at the contact. As a future improvement, spiked soles or a different setup height could be used to allow testing at angles greater than 40°.

The effect of the input platform angle proves to be fundamental to simulate the conditions close to real-world loads. Indeed, it significantly affects the $\tilde{F}_y / \tilde{F}_z$ trend, which is a crucial parameter to describe the conditions and the response that the foot prosthesis is experiencing during the stance phase.

The results presented in Table 2 suggest that, in the setup conditions presented, FR is less suitable for running at high speeds (above 5.5 m/s), as it is designed for jogging. The large discrepancy between CX and FR registered for User 2's run simulation indicates that CX performs better at higher inclination angles. During sprinting, the Center of Mass (CoM) shifts further forward than in jogging, requiring improved CX performance at steeper angles.

Indeed, the selected input lower platform angles are similar between the two models, but CX, particularly for User 2's simulation, shows a peak $\tilde{F}_y$ that is 15% greater than that of FR. The results found in this study are in line with the manufacturers' recommendations. Indeed, during sprinting and jumping, for which the use of CX is recommended, users seek greater forward push performance from the blade.

Supporting this, marker tracking reveals that when CX is compressed, its deformation causes the prosthetic pylon at the upper distal end to tilt approximately 45% more than FR, further enhancing the push forward (Fig. 10).

The experimental results confirm that this approach effectively replicates the conditions experienced by the prosthesis during the specified running gait. However, the inability to match the exact timing of a real run limits the precise reproduction of real running conditions. Applying the vertical load over a longer time interval than in real sprinting may lead to an underestimation of the peak forces, as the acceleration-related inertial effects are reduced. In addition, the lower strain rate may result in a softer mechanical response compared to the higher-speed conditions. Additionally, to prevent slippage at steep platform inclinations, spike soles can be introduced.

One limitation of the current setup is the 150 mm piston stroke, which requires modifications for certain tests. Additionally, this study only considers sagittal motion. A future step will be incorporating 3D motion, as the setup does not allow movement in the transverse plane.

Despite these constraints, the strong correlation between real-world running data and machine test results in terms of load validation is highly promising.

The method presented requires preliminary evaluations before conducting dynamic tests, but it enables the identification of platform angle trends for each RSP to simulate any specific running gait. Moving forward, the goal is to standardize the testing procedure by defining a reference running gait and establishing standardized input values. These values will vary based on the prosthesis model and be scaled according to stiffness properties.

Funding Open access funding provided by Politecnico di Torino within the CRUI-CARE Agreement.

Open Access This article is licensed under a Creative Commons Attribution 4.0 International License, which permits use, sharing, adaptation, distribution and reproduction in any medium or format, as long as you give appropriate credit to the original author(s) and the source, provide a link to the Creative Commons licence, and indicate if changes were made. The images or other third party material in this article are included in the article's Creative Commons licence, unless indicated otherwise in a credit line to the material. If material is not included in the article's Creative Commons licence and your intended use is not permitted by statutory regulation or exceeds the permitted use, you will need to obtain permission directly from the copyright holder. To view a copy of this licence, visit http://creativecommons.org/licenses/by/4.0/.

References

1. Dyer B, Sewell P, Noroozi S (2013) How should we assess the mechanical properties of lower-limb prosthesis technology used in elite sport?–an initial investigation. J Biomed Sci Eng 06:116–123. https://doi.org/10.4236/jbise.2013.62015
2. Dyer BTJ, Sewell P, Noroozi S (2014) An investigation into the measurement and prediction of mechanical stiffness of lower limb prostheses used for running. Assist Technol 26:157–163. https://doi.org/10.1080/10400435.2014.888599
3. McGowan CP, Grabowski AM, McDermott WJ, Herr HM, Kram R (2012) Leg stiffness of sprinters using running-specific prostheses. J R Soc Interface 9:1975–1982. https://doi.org/10.1098/rsif.2011.0877
4. Hobara H, Baum BS, Kwon H-J, Miller RH, Ogata T, Kim YH, Shim JK (2013) Amputee locomotion: Spring-like leg behavior and stiffness regulation using running-specific prostheses. J Biomech 46(14):2483–2489. https://doi.org/10.1016/j.jbiomech.2013.07.009
5. Barnett CT, Asha ARD, Skervin TK, Buckley JG, Foster RJ (2022) Spring-mass behavioural adaptations to acute changes in prosthetic blade stiffness during submaximal running in unilateral transtibial prosthesis users. https://doi.org/10.1016/j.gaitpost.2022.09.008
6. Beck ON, Taboga P, Grabowski AM, Beck ON (2017) Prosthetic model, but not stiffness or height, affects the metabolic cost of running for athletes with unilateral transtibial amputations.

J Appl Physiol 123:38–48. https://doi.org/10.1152/japplphysiol.00896.2016.-Run
7. Guzelbulut C, Suzuki K, Shimono S, Hobara H (2021) Effects of prosthetic design parameters on running performance of a unilateral transfemoral amputee. J Biomech Sci Eng 16:1–11. https://doi.org/10.1299/jbse.21-00023
8. Tacca JR, Beck ON, Taboga P, Grabowski AM (2022) Running-specific prosthesis model, stiffness and height affect biomechanics and asymmetry of athletes with unilateral leg amputations across speeds. Royal Soc Open Sci 9. https://doi.org/10.1098/rsos.211691
9. Rigney SM, Simmons A, Kark L (2016) A prosthesis-specific multi-link segment model of lower-limb amputee sprinting. J Biomech 49:3185–3193. https://doi.org/10.1016/j.jbiomech.2016.07.039
10. Beck ON, Taboga P, Grabowski AM (2016) Characterizing the mechanical properties of running-specific prostheses. PLoS ONE 11. https://doi.org/10.1371/journal.pone.0168298
11. Doyen S, F., Semblat, J.F. (2023) A novel characterisation protocol of mechanical interactions between the ground and a tibial prosthesis for long jump. Sci Rep 13. https://doi.org/10.1038/S41598-023-31981-2
12. Rigney SM, Simmons A, Kark L (2017) Mechanical characterization and comparison of energy storage and return prostheses. Med Eng Phys 41:90–96. https://doi.org/10.1016/j.medengphy.2017.01.003
13. Noroozi S, Ong ZC, Khoo SY, Aslani N, Sewell P (2019) Dynamic characterisation of Össur flex-run prosthetic feet for a more informed prescription. Prosthet Orthot Int 43:62–70. https://doi.org/10.1177/0309364618789449
14. 168, TCI (2016) ISO 10328:2016, Prosthetics — structural testing of lower-limb prostheses — requirements and test methods, p 139
15. 168, TCI (2016) ISO/TS 16955:2016, Prosthetics — quantification of physical parameters of ankle foot devices and foot units, 1st ed., p 17
16. 168, TCI (2024) ISO 22675:2024, Prosthetics — testing of ankle-foot devices and foot units — requirements and test methods, 3rd ed, p 91
17. Association, AOP (2010) What it is, what it is not, and what patient care facility providers/practitioners need to know…. Technical report
18. Barattini C, Dimauro L, Vella AD, Vigliani A (2024) Finite element model updating applied to a lower limb prosthesis through the optimisation of its mechanical properties. In: The international conference of IFToMM ITALY. Springer, pp 11–18
19. Noroozi S, Rahman AGA, Dupac M, Vinney JE (2012) Dynamic characteristics of prosthetic feet: A comparison between modal parameters of walking, running and sprinting foot, vol. 8. Springer, ???, pp 339–344. https://doi.org/10.1007/978-94-007-5125-5_44
20. Noroozi S, Sewell P, Rahman AGA, Vinney J, Chao OZ, Dyer B (2013) Modal analysis of composite prosthetic energy-storing-and-returning feet: An initial investigation. Proc Inst Mech Eng Part P J Sports Eng Technol 227:39–48. https://doi.org/10.1177/1754337112439274
21. Grobler L, Ferreira S, Vanwanseele B, Terblanche EE (2017) Characterisation of the responsive properties of two running-specific prosthetic models. Prosthet Orthot Int 41:141–148. https://doi.org/10.1177/0309364616660249
22. Hu M, Kobayashi T, Hisano G, Murata H, Ichimura D, Hobara H (2023) Sprinting performance of individuals with unilateral transfemoral amputation: compensation strategies for lower limb coordination. Royal Soc Open Sci 10. https://doi.org/10.1098/rsos.221198
23. Baum BS, Hobara H, Koh K, Kwon HJ, Miller RH, Shim JK (2019) Amputee locomotion: Joint moment adaptations to running speed using running-specific prostheses after unilateral transtibial amputation. Am J Phys Med Rehabil 98:182–190. https://doi.org/10.1097/PHM.0000000000000905
24. Cheetah Xceed, Össur. Model Overview and Specifications. https://www.ossur.com/en-au/prosthetics/feet/cheetah-xceed Accessed 17 Jan 2025
25. Flex Run, Össur. Model Overview and Specifications. https://www.ossur.com/en-us/prosthetics/feet/flex-run Accessed 17 Jan 2025
26. Össur: Instructions for Use: Flex-Foot Cheetah,Cheetah Xcel, Cheetah Xtend, Cheetah Xtreme, Cheetah Xpanse, Cheetah Junior. https://media.ossur.com/ossur-dam/image/upload/pi-documents-global/FLEX-FOOT_CHEETAH_CHEETAH_XCELCHEETAH_XTENDCHEETAH_XTREME_CHEETAH_XPANSE_CHEETAH_JUNIOR__1508_001_3.pdf. Accessed: 2024-12-31 (2015)
27. Grabowski AM, McGowan CP, McDermott WJ, Beale MT, Kram R, Herr HM (2010) Running-specific prostheses limit ground-force during sprinting. Biol Let 6:201–204. https://doi.org/10.1098/RSBL.2009.0729

Publisher's Note Springer Nature remains neutral with regard to jurisdictional claims in published maps and institutional affiliations.